17th World Conference on Earthquake Engineering, 17WCEE
Sendai, Japan - September 13th to 18th 2020

SEQUENTIAL EXPERIMENTAL DESIGN OF HYBRID SIMULATIONS FOR BAYESIAN CALIBRATION OF COMPUTATIONAL SIMULATORS

G. Abbiati[(1)], S. Marelli[(2)]

[(1)] *Assistant Professor, Department of Engineering, Aarhus University, Denmark, abbiati@eng.au.dk*
[(2)] *Senior Scientist, Chair of Risk, Safety and Uncertainty Quantification, ETH Zurich, Switzerland, marelli@ibk.baug.ethz.ch*

Abstract

Hybrid simulation combines physical and numerical substructures interacting with each other in a real-time control loop to simulate the time history response of a prototype structure subjected to a realistic excitation. Research on hybrid simulation is limited to the coupling of physical experiments and numerical simulations, that is, ensuring compatibility and balance of interface quantities involved by the physics of the prototype structure. No effort has been made yet to link experimental design and hybrid simulation. experimental design can be broadly defined as the process of selecting a particular setup for an experiment, from the parameter space of all the admissible setups, so as to maximize the information obtained from a future experiment prior to data collection. From a hybrid simulation perspective, the experimental design includes the definition of numerical substructures and loading excitations. From this standpoint, this paper presents an experimental design procedure that aims at maximizing the convergence rate of the Bayesian calibration of a computational simulation against hybrid simulation experiments.

Keywords: Hybrid simulation, experimental design, model calibration, Kriging surrogate modeling.

1 Introduction

An intrinsic component for achieving predictive maturity is model calibration, a methodology used to infer both the uncertain input parameters and the discrepancy bias of a computational simulation (CS), normally achieved through a systematic comparison of model predictions against experiments [1]. The shift from prescriptive to performance-based earthquake engineering motivated the development of hybrid simulation (HS) from the early 70s to reduce the cost of experimental testing for model calibration. HS combines physical and numerical substructures (PS and NS, respectively) interacting with each other in a real-time control loop to simulate the time history response of a prototype structure subjected to a realistic excitation [2]. Note that CSs are not expected to reproduce the entire range of possible behaviors of the corresponding real system, as the physics of a given structure is unlikely to be known at all scales and in all contexts. One only needs CSs that are accurate in a context of interest (e.g., range of boundary conditions) [3]. From this perspective, HS allows for covering such a context of interest by adjusting the parameters of the NS and the loading excitation, without additional implementation effort compared to the realization of a single experiment.

It is convenient to introduce here the concept of experimental design [4]. Experimental design can be defined as the process of optimizing the setting of an experiment to maximize an appropriate measure of information gain prior to data collection. Sequential experimental design (SED) indicates that such an optimization is repeated for each experiment of a batch based on previously collected data. From a HS perspective, SED can rely on a parametrization of NS and loading excitation. This is the basic assumption behind the HS-SED procedure presented in this paper. In principle, the proposed HS-SED procedure is driven by the Bayesian calibration of a CS against HS experiments. After every HS experiment, a Kriging surrogate model of a discrepancy norm between CS and HS response quantities of interest is trained [5]. The key for using a Kriging surrogate model is that it provides predictions of both average value and standard deviation of the discrepancy norm within the entire domain of variable input parameters defining the setting of the HS. The next sample of variable input parameters is selected such that the expected improvement of the discrepancy

norm is maximized [6]. This strategy ensures the exploration of subdomains where the uncertainty of the discrepancy norm is large, as well as the exploitation of subdomain where the expected value of the discrepancy norm predicted by the Kriging surrogate is large.

Surrogate modeling already showed promising results in enabling uncertainty propagation analysis, global sensitivity analysis [7] and reliability analysis [8] in HS applications, correcting the bias of ab initio CSs [9] and optimization of experimental setups [10]. The proposed methodology aims at contributing to make a leap in the current practice of quantification of structural response uncertainty advocated, e.g. by the opinion paper of Bradley [11].

2 Description of the sequential experimental design procedure

In the following, Section 2.1 provides the mathematical setting of Bayesian calibration. Basics of Kriging surrogate modeling are given in Section 2.2. Finally, Section 2.3 describes the proposed HS-SED procedure.

2.1 Basics of Bayesian calibration

According to the framework proposed by [12], in the process of model calibration, one must distinguish between two groups of input parameters. One group comprises input parameters that can be arbitrarily adjusted during the experiment (e.g., amplitude and frequency of the loading excitation), which are referred to as *variable inputs* and indicated with $\boldsymbol{x}$. The other group comprises the input parameters that we wish to learn from experimental data (e.g., material properties of the PS), which are referred to as *calibration parameters* and indicated with $\boldsymbol{\theta}$. Accordingly, the model calibration problem we wish to solve reads,

$$\mathcal{R}_{HS,j}(\boldsymbol{x}_i) = \mathcal{R}_{CS,j}\,(\boldsymbol{x}_i, \boldsymbol{\theta}) + \epsilon_j \tag{1}$$

where $\mathcal{R}_{HS,j}(\boldsymbol{x}_i)$ is the experimental response quantity of index j-th measured from the HS of index i-th, $\mathcal{R}_{CS,j}\,(\boldsymbol{x}_i, \boldsymbol{\theta})$ denotes the corresponding prediction provided by a CS, ϵ_j is the model discrepancy function, which possibly includes experimental errors (e.g., measurement noise). Model discrepancy results from missing physics and other inaccuracies of the structural simulator. Identifying the discrepancy function is important because it allows one to: i) learn the true value of the calibration parameters; ii) better understand deficiencies of the structural simulator. Bayesian inversion is used to compute posterior distributions of calibration parameters and model discrepancy given a set of measured experimental response quantities. For the sake of simplicity, we consider an additive Gaussian discrepancy with zero mean and given variance Σ_j,

$$\boldsymbol{\epsilon}_j \sim \mathcal{N}(\epsilon_j | 0, \Sigma_j). \tag{2}$$

In the context of model calibration, the goal is to find the optimal values of the calibration parameters $\boldsymbol{\theta}$ that allows one to fit the model predictions to the observations. In this respect, the epistemic uncertainty (lack of knowledge) on the calibration parameters is modeled by considering it as a random vector $\boldsymbol{\Theta} \sim \pi(\boldsymbol{\theta})$. From Eqs. (1-2) a particular measurement $\mathcal{R}_{HS,j}(\boldsymbol{x}_i)$ is a realization of a Gaussian distribution of mean value $\mathcal{R}_{CS,j}\,(\boldsymbol{x}_i, \boldsymbol{\theta})$ and variance Σ_j. Accordingly, the likelihood function, as a function of the calibration parameters $\boldsymbol{\theta}$, thus reads,

$$\mathcal{L}\left(\boldsymbol{\theta}; \mathcal{R}_{HS,j}(\boldsymbol{x}_i)\right) = \frac{1}{\sqrt{2\pi\Sigma_j^2}} \exp\left[-\frac{\left(\mathcal{R}_{HS,j}(\boldsymbol{x}_i) - \mathcal{R}_{CS,j}\,(\boldsymbol{x}_i, \boldsymbol{\theta})\right)^2}{2\Sigma_j^2}\right]. \tag{3}$$

If N independent experiments are performed, each with M response quantities of interest and measurements, the likelihood can be written as,

$$\mathcal{L}\left(\boldsymbol{\theta}; \boldsymbol{\mathcal{R}}_{HS}(\boldsymbol{x})\right) = \prod_{i=1}^{N} \prod_{j=1}^{M} \quad . \tag{4}$$

© The 17th World Conference on Earthquake Engineering

Where $\boldsymbol{\mathcal{R}}_{HS}(\boldsymbol{x})$ must be intended as the full set of $N \times M$ experimental observations. Combining the prior $\boldsymbol{\Theta} \sim \pi(\boldsymbol{\theta})$ and the likelihood $\mathcal{L}(\boldsymbol{\theta}; \boldsymbol{\mathcal{R}}_{HS}(\boldsymbol{x}))$ distributions through Bayes' theorem, the posterior distribution establishes the solution of the inverse problem,

$$\pi(\boldsymbol{\theta}|\boldsymbol{\mathcal{R}}_{HS}(\boldsymbol{x})) = \frac{1}{Z}\pi(\boldsymbol{\theta})\mathcal{L}(\boldsymbol{\theta}; \boldsymbol{\mathcal{R}}_{HS}(\boldsymbol{x})) \tag{5}$$

Where the normalizing factor Z, known as evidence or marginal likelihood, ensures that this distribution integrates to 1. The *maximum a posteriori* (MAP) estimate of $\boldsymbol{\theta}$ reads,

$$\boldsymbol{\theta}_{MAP} = \arg\max_{\boldsymbol{\theta}} \pi(\boldsymbol{\theta}|\boldsymbol{\mathcal{R}}_{HS}(\boldsymbol{x})). \tag{6}$$

In this work Bayesian inversion was performed using the UQLab software framework developed by the Chair of Risk, Safety and Uncertainty Quantification in ETH Zurich [13].

2.2 Basic of Kriging metamodeling

Kriging is a surrogate modeling technique that considers the computational model to be a realization of a Gaussian process [5]:

$$\widehat{\mathcal{M}}(\boldsymbol{x}) = \boldsymbol{\beta}^T \boldsymbol{f}(\boldsymbol{x}) + \sigma^2 Z(\boldsymbol{x}, \omega) \tag{7}$$

where $\boldsymbol{f}(\boldsymbol{x}) = [f_1(\boldsymbol{x}), \dots, f_p(\boldsymbol{x})]$ is a set of regression functions, $\boldsymbol{\beta}$ is a vector of coefficients, $Z(\boldsymbol{x}, \omega)$ is a zero-mean, unit-variance, stationary Gaussian process, and, σ^2 is the variance of the process. $Z(\boldsymbol{x}, \omega)$ is characterized by an autocorrelation function $R(|\boldsymbol{x} - \boldsymbol{x}'|; \boldsymbol{\rho})$, where $\boldsymbol{\rho}$ is the vector of hyper-parameters of the autocorrelation function. The Kriging model is trained with a set of realizations $\boldsymbol{\mathcal{X}} = \{\boldsymbol{\chi}^{(i)}, i = 1, \dots, i_{max}\}$ and the corresponding responses of the simulator $\boldsymbol{\mathcal{Y}} = \{\mathcal{Y}^{(i)} = \mathcal{M}(\boldsymbol{\chi}^{(i)}), i = 1, \dots, i_{max}\}$, which together form the so-called training set $\{\boldsymbol{\mathcal{X}}, \boldsymbol{\mathcal{Y}}\}$. Kriging parameters are obtained by generalized least-squared solution:

$$\boldsymbol{\beta}(\boldsymbol{\rho}) = (\mathbf{F}^T \mathbf{R}^{-1} \mathbf{F})^{-1} \mathbf{F}^T \mathbf{R}^{-1} \boldsymbol{\mathcal{Y}} \tag{8}$$

$$\sigma_y^2(\boldsymbol{\rho}) = \frac{1}{N}(\boldsymbol{\mathcal{Y}} - \mathbf{F}\boldsymbol{\beta})^T \mathbf{R}^{-1} (\boldsymbol{\mathcal{Y}} - \mathbf{F}\boldsymbol{\beta}) \tag{9}$$

where $\mathbf{R}_{ik} = R(|\boldsymbol{\chi}^{(i)} - \boldsymbol{\chi}^{(k)}|; \boldsymbol{\rho})$ is the correlation matrix and $\mathbf{F}_{il} = f_l(\boldsymbol{\chi}^{(i)})$. In order to cope with control and measurement errors, which make HS experiments stochastic even when the PS is undamaged, a small nugget is added to the diagonal of the correlation matrix and all hyper-parameter values are estimated via maximum likelihood. Having determined the Kriging parameters, the prediction value of the simulator at a test point $\boldsymbol{x} \in \mathcal{D}_X$ is a Gaussian variable with the following mean value and variance:

$$\mu_{\hat{Y}}(\boldsymbol{x}) = \boldsymbol{f}(\boldsymbol{x})^T \boldsymbol{\beta} + \boldsymbol{r}(\boldsymbol{x})^T \mathbf{R}^{-1} (\boldsymbol{\mathcal{Y}} - \mathbf{F}\boldsymbol{\beta}) \tag{10}$$

$$\sigma_{\hat{Y}}(\boldsymbol{x}) = \sigma_y^2 (1 - \boldsymbol{r}(\boldsymbol{x})^T \mathbf{R}^{-1} \boldsymbol{r}(\boldsymbol{x}) + \boldsymbol{u}(\boldsymbol{x})^T (\mathbf{F}^T \mathbf{R}^{-1} \mathbf{F})^{-1} \boldsymbol{u}(\boldsymbol{x})) \tag{11}$$

where $r_i(\boldsymbol{x}) = R(|\boldsymbol{x} - \boldsymbol{\chi}^{(i)}|; \boldsymbol{\rho})$ and $\boldsymbol{u}(\boldsymbol{x}) = \mathbf{F}^T \mathbf{R}^{-1} \boldsymbol{r}(\boldsymbol{x}) - \boldsymbol{f}(\boldsymbol{x})$. The trained Kriging model, produced by the process above supports the adaptive design of experiments described in the following section. In this work, Kriging surrogate models were estimated using the UQLab software framework developed by the Chair of Risk, Safety and Uncertainty Quantification in ETH Zurich [13].

2.3 Adaptive design of experiments

In this study, $\boldsymbol{x}$ represents the vector of the variable input parameters, which can be controlled in the HS, whereas $\mathcal{M}(\boldsymbol{x})$ is a function that measures the discrepancy between HS and CS over a set of response quantities of index j,

$$y = \mathcal{M}(\boldsymbol{x}) = \sum_j \frac{\left(\mathcal{R}_{HS,j}(\boldsymbol{x}) - \mathcal{R}_{CS,j}(\boldsymbol{x}, \boldsymbol{\theta}_{MPA})\right)^2}{Var_{\boldsymbol{x},\boldsymbol{\theta}}[\mathcal{R}_{CS,j}(\boldsymbol{x}, \boldsymbol{\theta}_{MAP})]} \tag{12}$$

© The 17th World Conference on Earthquake Engineering

For a given set of samples $\boldsymbol{x}_i \in \boldsymbol{\mathcal{X}}$ of the input parameter vector $y_i \in \boldsymbol{\mathcal{Y}}$ provide the complete training set $\{\boldsymbol{\mathcal{X}}, \boldsymbol{\mathcal{Y}}\}$ for the Kriging metamodel $\widehat{\mathcal{M}}(\boldsymbol{x})$. Accordingly, the expected improvement algorithm [6] is used to find the regions of the maximum discrepancy between the response of the HS and the CS updated based on all previous experiments.

$$\boldsymbol{x}^* = \arg\max_{\boldsymbol{x}} \widehat{\mathcal{M}}(\boldsymbol{x}). \tag{13}$$

In the following, the proposed HS-SED procedure is introduced as a sequence of steps:

1. Generate a small initial realization $\boldsymbol{\mathcal{X}} = \{\boldsymbol{x}_i, i = 1, \dots, N_{ini}\}$ of the variable input vector and evaluate $\mathcal{R}_{HS,j}(\boldsymbol{x}_i)$ via HS.
2. Compute/update the posterior distribution of the calibration parameters $\boldsymbol{\theta}$ via Bayesian inversion by using $\mathcal{R}_{CS,j}(\boldsymbol{x}_i, \boldsymbol{\theta})$, as forward models as explained in Section 2.1.
3. Compute $\boldsymbol{\mathcal{Y}} = \mathcal{M}(\boldsymbol{\mathcal{X}})$, which together form the initial training set $\{\boldsymbol{\mathcal{X}}, \boldsymbol{\mathcal{Y}}\}$.
4. Train a Kriging surrogate model $\widehat{\mathcal{M}}(\boldsymbol{x})$ based on the relevant training set $\{\boldsymbol{\mathcal{X}}, \boldsymbol{\mathcal{Y}}\}$ as explained in Section 2.2
5. Generate a large set $\mathcal{S} = \{\boldsymbol{x}_1, \dots \boldsymbol{x}_n\}$ from the space of variable input $\boldsymbol{x}$ and compute the response of $\widehat{\mathcal{M}}(\boldsymbol{x})$, i.e. $\mu_{\hat{y}}(\boldsymbol{x})$ and $\sigma_{\hat{y}}(\boldsymbol{x})$.
6. Enrich the training set by selecting the sample $\boldsymbol{x}^* \in \mathcal{S}$ that, among all metamodels $\widehat{\mathcal{M}}(\boldsymbol{x})$, maximize the expected value of the so-called "improvement random variable", $I(\boldsymbol{x}) = \max\left(\hat{y}(\boldsymbol{x}) - \mu_{\hat{y}_{max}}, 0\right)$,

$$\{\boldsymbol{x}^*\} = \arg\max_{\boldsymbol{x}} E[I(\boldsymbol{x})] =$$
$$= \arg\max_{\boldsymbol{x}} \left(\mu_{\hat{y}}(\boldsymbol{x}) - \mu_{\hat{y}_{max}}\right)\left[1 - \Phi\left(\frac{\mu_{\hat{y}_{max}} - \mu_{\hat{y}}(\boldsymbol{x})}{\sigma_{\hat{y}}(\boldsymbol{x})}\right)\right] + \sigma_{\hat{y}}(\boldsymbol{x})\phi\left(\frac{\mu_{\hat{y}_{max}} - \mu_{\hat{y}}(\boldsymbol{x})}{\sigma_{\hat{y}}(\boldsymbol{x})}\right) \tag{14}$$

   where $\Phi(\cdot)$ and $\phi(\cdot)$ are CDF and PDF of a standard Gaussian variable. The expected improvement method locates samples by using a tradeoff between the exploration of regions where Kriging variance predictors are higher and the exploitation of regions function where Kriging average predictors are higher.

7. Evaluate $\mathcal{R}_{HS,j}(\boldsymbol{x}^*)$ via HS.
8. Loop between Step #2 and #7 until the maximum number of iterations is reached.

If $\mu_{\hat{y}_{max}}$ converge rapidity to true global maximum values, then the proposed procedure represents a compelling and attractive method to minimize the number of HSs while increasing the relevance of benchmarks for calibration of CSs.

3 Verification of the experimental design procedure

3.1 The benchmark case study

The 2-Degrees-of-Freedom (DoFs) system depicted in Fig. 2 was selected for benchmarking the proposed experimental design procedure.

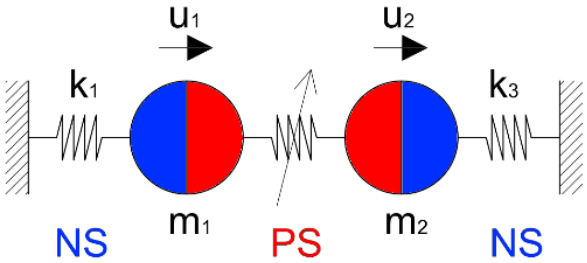

Fig. 1 – Hybrid simulator (HS).

© The 17th World Conference on Earthquake Engineering

As shown in Fig. 2, a nonlinear spring connecting the two masses represents the PS. Linear elastic springs k_1 and k_3 are constrained to the ground and belong to the NS while masses m_1 and m_2 are split between the two subdomains. In the real case, the PS spring would be tested in a laboratory, but in this study, its force-deformation response is modeled numerically using a Bouc-Wen model with stiffness deterioration [14]. The following ODE set describes the nonlinear restoring force of the middle spring,

$$\begin{cases} \dot{r} = \dfrac{A_{ref} - \left(\beta_{ref}\,\mathrm{sign}(\Delta\dot{u}\cdot r) + \gamma_{ref}\right)|r|^{n_{ref}}}{1+\eta_{ref}e}\Delta\dot{u} \\ \dot{e} = r\cdot\Delta\dot{u} \end{cases} \tag{15}$$

Where r and $\Delta u = u_2 - u_1$ indicate spring restoring force and elongation, respectively. Reference parameters $A_{ref}, \beta_{ref}, \gamma_{ref}$ and n_{ref} refers to the Bouc-Wen model whereas the parameter η_{ref} modulates stiffness deterioration, which is assumed to be proportional to the hysteretic energy e dissipated by the nonlinear spring. The values of the parameters of the 2-DoFs nonlinear HS read,

$$m_1 = 8e3\ kg, m_2 = 9e3\ kg, k_1 = 4e5\frac{N}{m}, k_3 = 1e6\frac{N}{m}, \zeta = 0.05$$

$$A_{ref} = 5e5\frac{N}{m}, \beta_{ref} = 1, \gamma_{ref} = 0, \eta_{ref} = 2e-5, n_{ref} = 1$$

The undamped eigenfrequencies of the 2-DoFs system linearized about the initial (unreformed) configuration are 1.38 Hz and 2.34 Hz. A uniform modal damping $\zeta = 0.05$ is assumed for the calculation of the damping matrix. A simpler variant of Eq. (15), which corresponds to a classical Bouc-Wen spring without stiffness degradation, describes the PS restoring force of the CS, which is reported in Fig. 2. This choice reflects the fact that a computational model is a simplified representation of a real system, and therefore it does not completely capture its behavior.

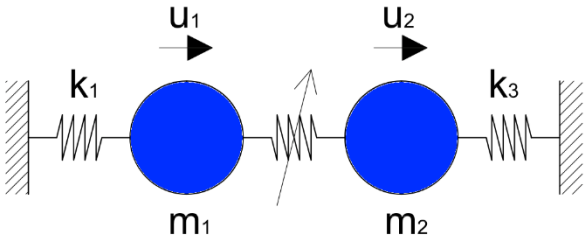

Fig. 2 – Computational simulator (CS).

In earthquake engineering, it is common practice to consider the variability of the ground motion predominant with respect to all other sources of uncertainty (e.g., material parameters or boundary conditions). Accordingly, in this study, the near-fault pulse model of Dabaghi and Der Kiureghian [15] is selected to parametrize the seismic excitation, and therefore, the context of interest for model calibration whereas NS parameters are assumed as deterministic. The following equations define the shape of the velocity pulse in the time domain,

$$v_{pul}(t) = \left\{\frac{1}{2}V_P cos\left[2\pi\left(\frac{t-t_{max}}{T_P}\right)+\nu\right] - \frac{D_r}{\gamma T_P}\right\}\left\{1+cos\left[\frac{2\pi}{\gamma}\left(\frac{t-t_{max}}{T_P}\right)\right]\right\} \tag{16}$$

$$D_r = V_P T_P \frac{sin(\nu+\gamma\pi) - sin(\nu-\gamma\pi)}{4\pi(1-\gamma^2)} \tag{17}$$

where V_P and T_P are velocity peak and duration of the pulse, γ is the number of oscillations within the pulse and ν is the phase angle between time modulating function and pulse oscillations. The seismic accelerogram $a_g(t)$ is found as the time derivative of the velocity pulse. A preliminary global sensitivity

© The 17th World Conference on Earthquake Engineering

analysis highlighted a negligible sensitivity of the 2-DoFs system response to parameters γ and ν. Therefore, V_P and T_P are selected as variable inputs. Related PDFs are summarized in Table 1.

Table 1 - Intervals of variable input $\mathbf{x} = \{V_P, T_P\}$.

Label	PDF	Lower bound	Upper bound
V_P	Uniform	1.5 m/s	3.0 m/s
T_P	Uniform	0.5 s	1.5 s

Constant values are assumed for $\gamma = 2.00$ and $\nu = 0.10$ [rad/s]. For the sake of example, Fig. 3 depicts 1000 ground motion realizations as well as related response spectra assuming the same damping ratio of the 2-DoFs system, which is equal to 0.05.

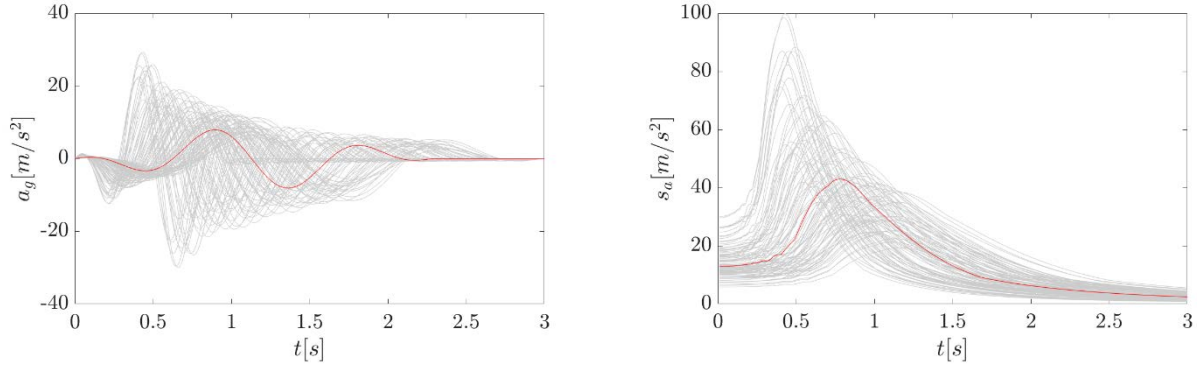

a b

Fig. 3 - Pulse-like ground motion model: a) acceleration histories and b) acceleration response spectra. Grey curves correspond to 1000 random realization while red curves refer to average values of ground motion parameters (VP = 2.25 m/s; TP = 1.00 s).

Fig. 4 compares the dynamic responses of HS and CS subjected to the accelerogram highlighted in red in Fig. 3, which corresponds to the average values of ground motion parameters.

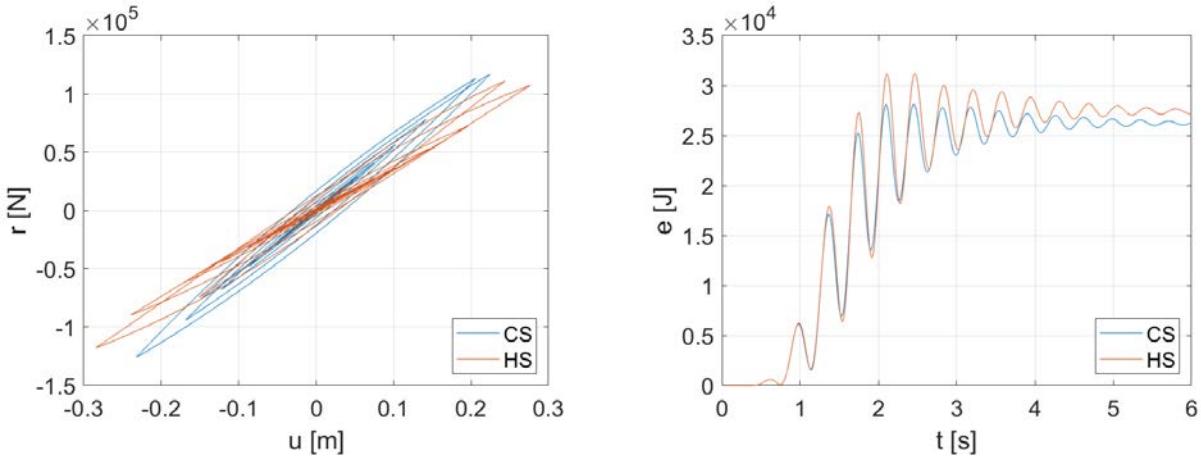

a b

Fig. 4 - Comparison between CS and HS responses computed considering average values of ground motion parameters (VP = 2.25 m/s; TP = 1.00 s): a) hysteresis loop and b) dissipated energy history of the nonlinear spring.

© The 17th World Conference on Earthquake Engineering

As can be appreciated from Fig. 4a, the HS shows stiffness degradation, which does not occur on the CS. It is important to stress that the proposed benchmark case study well represents the class of structural systems emulated via HS. In fact, two eigenmodes govern the dynamic response produced by the seismic loading, nonlinearities are confined to the PS.

3.2 Numerical simulation of the experimental campaign

The setting of the Bayesian calibration problem underlying the proposed experimental design procedure is determined by the following response quantities of interest,

$$\mathcal{R}_{HS,r}(\boldsymbol{x}) = \max_t |r| \,, \mathcal{R}_{HS,\Delta u}(\boldsymbol{x}) = \max_t |\Delta u| \,, \mathcal{R}_{HS,\mathrm{e}}(\boldsymbol{x}) = e(\max(t)) \tag{18}$$

where labels $\Delta u, r$ and e absolute elongation peak, absolute restoring force peak and total dissipated energy of the nonlinear spring representing the PS. On the other hand, Table 2 reports the prior distribution of the calibration parameters s of the CS.

Table 2 – Prior distributions of the calibration parameters $\boldsymbol{\theta} = \{A, \beta\}$.

Label	PDF	Lower bound	Upper bound
A	Uniform	2e5 N/m	9e5 N/m
β	Uniform	0.5	2.0

As a measure of model inadequacy, contour plots of Fig. 4 shows the MAP estimates of both calibration parameters $\boldsymbol{\theta} = \{A, \beta\}$ computed via Bayesian inversion and considering a single HS evaluation taken from the corresponding pair of variable inputs $\boldsymbol{x} = \{V_P, T_P\}$.

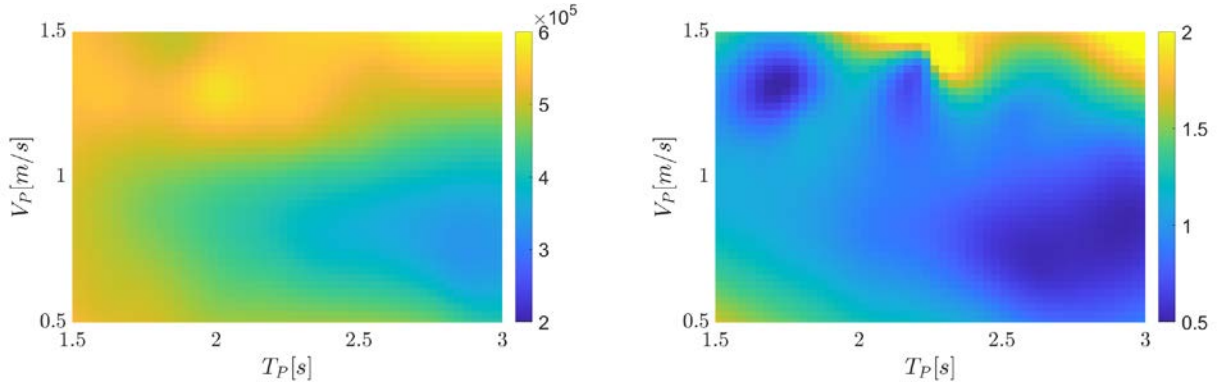

Fig. 4 - MAP estimates of calibration parameters of the CS computed considering a single realization of the HS over the entire domain of variable input: a) A_{MAP}; b) β_{MAP}.

As can be appreciated from Fig. 4, both calibration parameters MAP estimates show a large variability over the domain of variable input. This is a clear example of how model inadequacy causes overfitting of calibration parameters. For this reason, it is of paramount importance to gather experimental observations over the entire domain of variable input, which defines a context of engineering interest where a calibrated model is sought.

According to Step #1 of the experimental design procedure, an initial training set of three samples is generated by sampling the input parameter space of the ground motion model with a Sobol sequence [16] and evaluating the corresponding responses of both HS and CS. Then, the training set is adaptively enriched by iterating the HS-SED procedure from Step #2 to #7 for 40 times. Fig. 5 reports the history of $\max_{\boldsymbol{x}} E[I(\boldsymbol{x})]$ at each iteration. The contour plot of Fig. 6 ranks the different regions of the domain of variable input based on

© The 17th World Conference on Earthquake Engineering

when they have been explored by the adaptive sampling. Regions characterized by a value close to zero have been explored during the first iterations whereas values close to one indicates that the region was explored toward the end of the procedure.

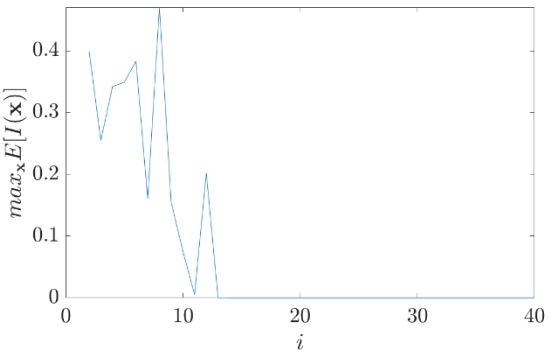

Fig. 5 – Maximum value of the expected improvement function $\max_{\boldsymbol{x}} E[I(\boldsymbol{x})]$.

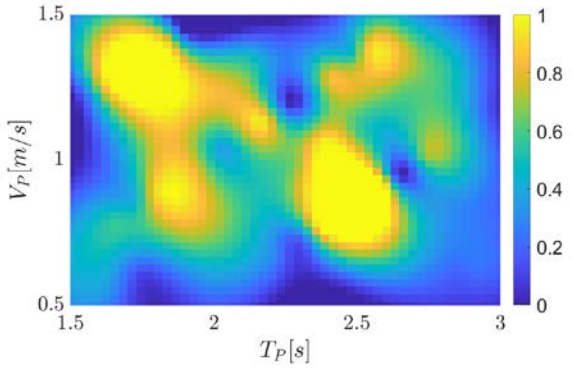

Fig. 6 – Mapping of sorting order of variable input samples: values close to 0 are explored firstly whereas values close to 1 are explored lastly.

According to Fig. 5, the maximum expected improvement of the discrepancy function stably approached zero right before 20 iterations. Fig. 7 shows the MAP estimates of calibration parameters s at each iteration of the HS-SED procedure.

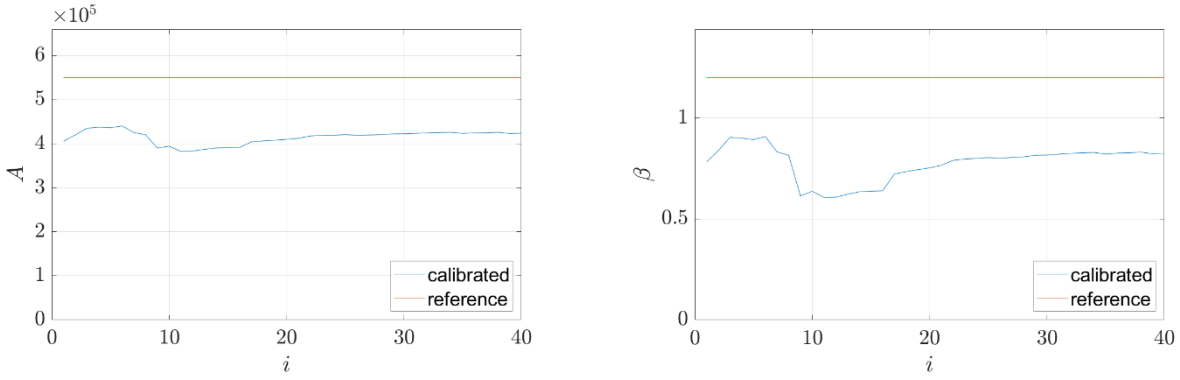

a b

Fig. 7 – MAP estimates of calibration parameters s: a) A_{MAP}; b) β_{MAP}.

As can be appreciated from Fig. 7, both calibration parameters achieved stable values right about 20 iterations, that is, when $\max_{\boldsymbol{x}} E[I(\boldsymbol{x})]$ already achieved stable convergence. For the sake of comparison, also the parameters of the nonlinear PS of the HS and reported in Section 3.1 are also reported and indicated as reference. As expected, the calibration parameters identified by using the simplified CS as a forward model are biased with respect to reference values.

In order to verify the effectiveness of the proposed HS-SED procedure, the response of the CS obtained considering the final MAP estimate of calibration parameters s ($A_{MAP} = 4.24e5, \beta_{MAP} = 0.826$) was compared to the response of the HS for two different samples of variable input parameters. In this regard, Fig. 8 gathers the responses obtained from the nonlinear spring, which is assimilated to the PS.

© The 17th World Conference on Earthquake Engineering

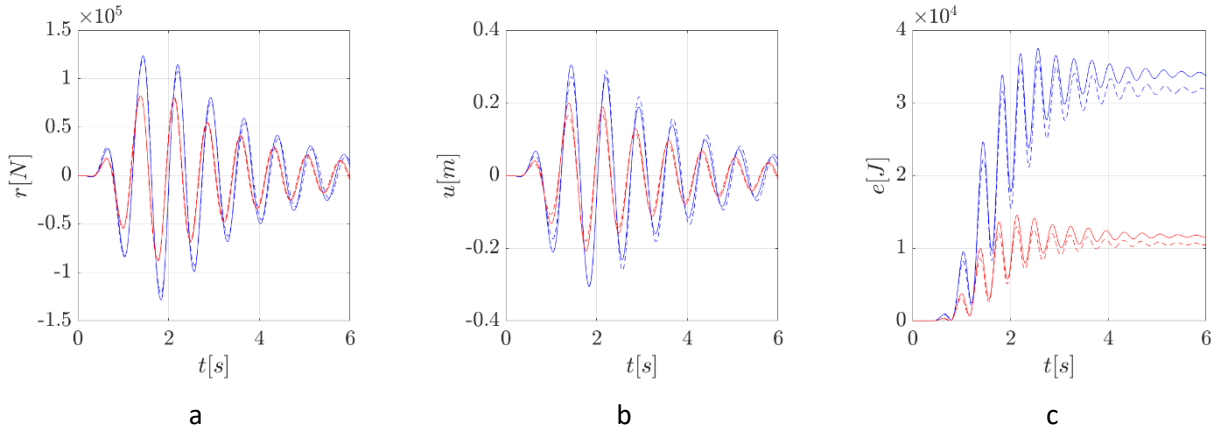

Fig. 8 – Comparison of calibrated CS (continuous lines) and HS (dashed lines) responses for two samples of variable input parameters ($V_{P,1} = 2.90, T_{P,1} = 1.09$ and $V_{P,1} = 1.68, T_{P,1} = 1.03$): a) restoring force; b) elongation; c) dissipated energy of the nonlinear spring (PS).

As can be appreciated from Fig. 8, the response of the calibrated CS provides a satisfactory agreement with the HS response for all quantity of interest.

4 Conclusions

This paper presented an experimental design procedure for hybrid simulations that aims at accelerating the convergence rate of an underlying model calibration problem. It is noteworthy that a calibrated model is not expected to reproduce the response of a corresponding real system within the entire range of possible loading scenarios but only for a limited context of interest. In the proposed procedure, the latter is explored by parametrizing the loading excitation used for hybrid simulation over a space of -controllable- variable input. A Kriging surrogate model of a norm of the model discrepancy between hybrid and computational simulation supports the experimental design. In detail, the next candidate sample of a variable input is selected such that it maximizes the expected improvement of the model discrepancy. The effectiveness of the proposed procedure is demonstrated for a virtual 2-DoFs case study considering a parametrized ground motion excitation.

5 Acknowledgments

The authors wish to acknowledge Dr. Marco Broccardo (University of Liverpool, UK) for his comments on the idea as well as the formulation of the benchmark case study.

6 References

[1] T. G. Trucano, L. P. Swiler, T. Igusa, W. L. Oberkamp and M. Pilch, "Calibration, validation, and sensitivity analysis: What's what.," *Reliability Engineering and System Safety*, vol. 91, no. 10-11, p. 1331–1357, 2006.

[2] A. Schellenberg, S. Mahin and G. Fenves, "Advanced Implementation of Hybrid Simulation," 2009.

[3] K. Worden, E. J. Cross, P. Gardner, R. J. Barthorpe and D. J. Wagg, "On Digital Twins, Mirrors and Virtualisations," in *Conference Proceedings of the Society for Experimental Mechanics Series*, 2020.

© The 17th World Conference on Earthquake Engineering

[4] R. A. Fisher, The Design of Experiments, Edinburgh: Oliver & Boyd, 1966.

[5] T. J. Santner, J. W. Brian and W. I. Notz, The design and analysis of computer experiments, Springer Science & Business Media, 2013.

[6] D. R. Jones, M. Schonlau and W. J. Welch, "Efficient global optimization of expensive black-box functions," *Journal of Global optimization,* vol. 13, no. 4, pp. 455-492, 1998.

[7] G. Abbiati, S. Marelli, O. S. Bursi, B. Sudret and B. Stojadinovic, "Uncertainty Propagation and Global Sensitivity Analysis in Hybrid Simulation Using Polynomial Chaos Expansion," in *Proceedings of the 15th International Conference on Civil, Structural and Environmental Engineering Computing CIVIL-SOFT-COMP (CSC2015)*, Prague, 2015.

[8] G. Abbiati, R. Schöbi, B. Sudret and B. Stojadinovic,, "Structural Reliability Analysis Using Deterministic Hybrid Simulations and Adaptive Kriging Metamodeling.," in *Proceedings of the 16th World Conference on Earthquake Engineering (16WCEE)*, Santiago, 2017.

[9] G. Abbiati, I. Abdallah, S. Marelli and B. Sudret, "Hierarchical Kriging Surrogate of the Seismic Response of a Steel Piping Network Based on Multi-Fidelity Hybrid and Computational Simulators," in *Proceedings of the 7th International Conference on Advances in Experimental Structural Engineering (7AESE)*, Pavia, 2017.

[10] T. Sauder, S. Marelli, K. Larsen and A. J. Sørensen, "Active truncation of slender marine structures: Influence of the control system on fidelity," *Applied Ocean Research,* vol. 74, pp. 154-169, 2018.

[11] B. A. Bradley, "A critical examination of seismic response uncertainty analysis in earthquake engineering," *Earthquake Engineering & Structural Dynamics,* vol. 42, no. 11, p. 1717–1729, 2013.

[12] M. C. Kennedy and A. O'Hagan, "Bayesian calibration of computer models," *Journal of the Royal Statistical Society B,* vol. 63, p. 425–64, 2001.

[13] S. Marelli and B. Sudret, "UQLab: A framework for uncertainty quantification in Matlab.," in *In Vulnerability, Uncertainty, and Risk (Proc. 2nd Int. Conf. on Vulnerability, Risk Analysis and Management (ICVRAM2014)*, Liverpool, 2014.

[14] M. Ismail, I. Fayçal and J. Rodellar, "The hysteresis Bouc-Wen model, a survey," *Archives of Computational Methods in Engineering,* vol. 16, no. 2, pp. 161-188, 2009.

[15] M. Dabaghi and A. Der Kiureghian, "Stochastic model for simulation of near‐fault ground motions," *Earthquake Engineering & Structural Dynamics,* vol. 46, no. 6, pp. 963-984, 2017.

[16] I. M. Sobol, "Distribution of points in a cube and approximate evaluation of integrals," *U.S.S.R Comput. Maths. Math. Phys.,* vol. 7, p. 86–112, 1967.

© The 17th World Conference on Earthquake Engineering